ORA Mathematics, 1(1), e2026004
DOI: 10.XXXXX/oramath.e2026004
Received: 20 April 2026
Revised: 03 May 2026
Accepted: 06 May 2026
Published: 08 May 2026

RESEARCH ARTICLE

Spectral distortion constrained reheating in a holographic induced gravity tachyon model under ACT observations

Khush Bakhat Liaqat *

Department of Mathematics, University of the Punjab, Lahore, Pakistan

* **Correspondence:** Email: khush.rubab21@gmail.com

Abstract: We present a Spectral Distortion Constrained Reheating (SDCR) analysis of tachyon inflation within the holographic induced gravity (H-IG) framework, using the latest observational data from the Atacama Cosmology Telescope (ACT) DR6 combined dataset P-ACT-LB-BK18, which yields $n_s = 0.9743 \pm 0.0034$. The model is characterized by three free parameters: the holographic parameter c, the induced gravity (IG) parameter γ, and the potential parameter α governing the exponential tachyon potential. Analytical expressions for the reheating temperature T_{re} and the reheating e-folds N_{re} are derived under a constant effective equation of state ω_{re}. We then impose CMB μ-type and y-type spectral distortion bounds as supplementary observational filters on the parameter space, alongside the standard n_s constraint. The energy injected into the photon-baryon plasma during reheating is computed for each parameter combination and compared against current FIRAS limits and projected PIXIE-class sensitivities. The Spectral Distortion Constrained Reheating method contracts the viable reheating corridor substantially relative to the base spectral index constraint alone, eliminating low-reheating-temperature branches that would otherwise survive n_s filtering. Numerical results show that the observationally preferred configuration corresponds to $\alpha \sim 2.5 \times 10^{-5}$, $c \sim 1 \times 10^{7}$, and $\gamma \sim 0.9$, consistent with instantaneous reheating near $T_{re} \sim 5 \times 10^{15}$ GeV. The spectral distortion filter independently reinforces this conclusion, with μ-distortion constraints ruling out $T_{re} \lesssim 10^4$ GeV for the matter-like equation-of-state branch.

Keywords: Tachyon inflation; Holographic induced gravity; Reheating temperature; CMB spectral distortions; ACT constraints; Exponential potential; Equation of state

Mathematics Subject Classification: 83F05, 85A40

1. Introduction

Inflation remains the leading paradigm for explaining the large-scale homogeneity, flatness, and the absence of unwanted relics in the observable Universe [14–16]. A period of accelerated expansion driven by a scalar or non-canonical field not only resolves the classical shortcomings of standard Big Bang cosmology but also seeds the primordial perturbations that develop into the large-scale structure seen today. Two pivotal observables — the scalar spectral index n_s and the tensor-to-scalar ratio r — encode the shape of the inflationary potential and serve as direct links between theory and CMB measurement [12, 13].

Recent data from the Atacama Cosmology Telescope (ACT) DR6, combined with Planck 2018, BICEP/Keck 2018, and DESI data (P-ACT-LB-BK18), yield $n_s = 0.9743 \pm 0.0034$,

representing a modest upward shift relative to the Planck-only value [10, 14]. This shift has non-trivial consequences for inflationary model building: potentials that were marginally consistent with Planck 2018 are now either confirmed or excluded, and the viable parameter space for post-inflationary dynamics is correspondingly refined.

Tachyon inflation, motivated by the open string theory Born–Infeld action, offers a geometrically distinct mechanism for driving inflation [2, 16]. The Dirac–Born–Infeld (DBI) structure of the tachyon Lagrangian prevents field oscillations around a potential minimum, so the transition from inflation to the radiation-dominated era does not proceed through the conventional inflaton-decay channel. Instead, the tachyon rolls monotonically toward vanishing potential energy, and reheating must be understood through the energy transfer encoded in the effective equation of state during this rolling phase. The exponential potential $V(\tilde{T}) = V_0 \exp(-\alpha\tilde{T}/\kappa_4)$ is particularly well-suited for this study, as it admits analytical slow-roll treatment and is compatible with string-theoretic estimates of the tachyon mass [6, 7].

Embedding tachyon inflation within the Randall–Sundrum type II (RSII) braneworld scenario, extended by holographic corrections and an induced gravity (IG) term, introduces two additional physical ingredients that alter the effective Friedmann dynamics at high energies [9, 16]. The holographic parameter c connects the four-dimensional and five-dimensional Planck masses, while the IG parameter γ controls the strength of the quantum-gravity correction to the effective gravitational coupling. Together, these ingredients define the Holographic Induced Gravity (H-IG) framework studied here.

When inflation ends, the Universe is cold and far from thermal equilibrium. For Big Bang nucleosynthesis (BBN) and baryogenesis to proceed, the Universe must thermalize, reaching a minimum reheating temperature $T_{re} \gtrsim 10$ MeV [3, 5]. The reheating phase is conventionally parametrized by three quantities: the reheating temperature T_{re}, the effective equation of state ω_{re}, and the duration N_{re} measured in e-folds. These quantities are not independent; they are tied to the inflationary observables through consistency relations that exploit the known expansion history between horizon exit and the onset of the radiation-dominated era [4, 10].

Most analyses of reheating constrain T_{re} and N_{re} using n_s and N_k alone. An independent and complementary observational handle comes from CMB spectral distortions [6, 11]. Energy injected into the photon-baryon plasma at redshifts $5 \times 10^4 \lesssim z \lesssim 2 \times 10^6$ produces μ-type distortions, while injections at $z \lesssim 5 \times 10^4$ generate y-type distortions. The FIRAS instrument aboard COBE placed the bounds $|\mu| < 9 \times 10^{-5}$ and $|y| < 1.5 \times 10^{-5}$ at 95% confidence, and next-generation experiments such as PIXIE and Voyage 2050 are projected to improve sensitivity by three to four orders of magnitude [1, 8].

In this work, we apply the Spectral Distortion Constrained Reheating (SDCR) method to the H-IG tachyon model with an exponential potential. For each combination of model parameters (c, α, γ) and equation-of-state value ω_{re}, we compute the fractional energy injection $\Delta\rho/\rho$ during reheating and compare it against FIRAS spectral distortion limits and projected PIXIE-class bounds. This additional filter eliminates branches of the parameter space that survive the n_s constraint but would produce distortions in conflict with observations. The method thereby provides a tighter and physically better motivated constraint on the reheating corridor than n_s alone.

The paper is structured as follows. Section 2 reviews the H-IG tachyon model, deriving the modified Friedmann equation, slow-roll parameters, inflationary observables, and their depen-

dence on the model parameters under P-ACT-LB-BK18 constraints. In Sec. 3, we derive the reheating relations which connect T_{re} and N_{re} to the inflationary quantities. In Section 4 we present the SDCR framework, including the spectral distortion energy injection formula, the FIRAS and PIXIE bounds, and how to apply them as filters on the H-IG parameter space. In section 5 we present the complete numerical analysis, contrasting results with and without the SDCR constraint (and the n_s filtering). We summarize the main results in Section 6.

2. Tachyon Field With H-IG Model And Inflationary Predictions

2.1. Modified Friedmann Equation And Field Dynamics

The H-IG framework rests on a holographic reformulation of the RSII braneworld model, augmented by an induced gravity correction. Within this setting, the effective Friedmann equation governing a tachyon field $\tilde{T}$ on the brane takes the form [16]

$$H^2 = \frac{1+\gamma}{4c\kappa_4^2}\left[1-\sqrt{1-\frac{\rho_{\tilde{T}}}{\rho_{\max}}}\right], \tag{1}$$

where $\gamma \in [0,1)$ is the dimensionless IG parameter, $c = 1/(\kappa_4^6 M^6)$ is the holographic parameter connecting the reduced four-dimensional Planck mass $\kappa_4^{-1} = 2.435 \times 10^{18}$ GeV and the five-dimensional Planck mass M, and $\rho_{\max} = 3(1+\gamma)^2/(8c\kappa_4^4)$ is the maximum energy density permitted in the model. The tachyon energy density is

$$\rho_{\tilde{T}} = \frac{V(\tilde{T})}{\sqrt{1-\dot{\tilde{T}}^2}}, \tag{2}$$

where $V(\tilde{T})$ is the tachyon potential and an overdot denotes differentiation with respect to cosmic time. The equation of motion for the tachyon field on the brane is

$$\frac{\ddot{\tilde{T}}}{1-\dot{\tilde{T}}^2} + 3H\dot{\tilde{T}} + \frac{V_{,\tilde{T}}}{V(\tilde{T})} = 0, \tag{3}$$

with $V_{,\tilde{T}} = dV/d\tilde{T}$.

2.2. Slow-Roll Approximation And Observable Parameters

Under the slow-roll approximation, $\dot{\tilde{T}}^2 \ll 1$ and $\ddot{\tilde{T}} \ll 3H\dot{\tilde{T}}$, Eqs. (1) and (3) simplify to

$$H^2 \simeq \frac{1+\gamma}{4c\kappa_4^2}\left[1-\sqrt{1-\chi(\tilde{T})}\right], \tag{4}$$

and

$$3H\dot{\tilde{T}} \simeq -\frac{V_{,\tilde{T}}}{V(\tilde{T})}, \tag{5}$$

where $\chi(\tilde{T}) = V(\tilde{T})/\rho_{\max}$ is a dimensionless ratio quantifying the proximity of the field energy to the holographic maximum. Standard four-dimensional general relativity is recovered when $\chi \ll 1$ and $\gamma = 0$.

The slow-roll parameters within the H-IG tachyon framework are [7, 16]

$$\epsilon_{\tilde{T}} \simeq \frac{1}{2\kappa_4^2}\frac{V_{,\tilde{T}}^2}{V(\tilde{T})^3}\,Q_1, \tag{6}$$

$$\eta_{\tilde{T}} \simeq \frac{1}{\kappa_4^2}\frac{V_{,\tilde{T}\tilde{T}}}{V(\tilde{T})^2}\,Q_2, \tag{7}$$

where the correction factors Q_1 and Q_2 encode the combined holographic and IG modifications,

$$Q_1 = \frac{(1+\gamma)\left[1+F(\chi)\right]^2}{4F(\chi)}, \qquad Q_2 = \frac{(1+\gamma)\left[1+F(\chi)\right]}{2}, \tag{8}$$

with $F(\chi) = \sqrt{1-\chi(\tilde{T})}$. Inflation ends when $\epsilon_{\tilde{T}}(\tilde{T}_{\rm end}) = 1$.

2.3. Exponential Potential And Inflationary Observables

The tachyon potential adopted throughout this study is the exponential form [4, 7]

$$V(\tilde{T}) = V_0 \exp\!\left(\frac{-\alpha}{\kappa_4}\tilde{T}\right), \tag{9}$$

where α and V_0 are free parameters, and α/κ_4 represents the tachyon mass with a typical estimate $\alpha \sim 10^{-5}$ [16]. The exponential form permits analytical progress in the slow-roll regime and ensures $V(\tilde{T}) \to 0$ as $\tilde{T} \to \infty$, providing a natural exit from inflation. The number of e-folds from CMB pivot-scale horizon crossing (field value $\tilde{T}_k$) to the end of inflation (field value $\tilde{T}_{\rm end}$) is

$$N_k = \frac{3(\gamma+1)}{2\alpha^2 c}\left[\ln\!\left(\frac{1+\sqrt{1-\chi_k}}{1+\sqrt{1-\chi_{\rm end}}}\right) + \sqrt{1-\chi_{\rm end}} - \sqrt{1-\chi_k}\right], \tag{10}$$

where $\chi_k \equiv \chi(\tilde{T}_k)$ and $\chi_{\rm end} \equiv \chi(\tilde{T}_{\rm end})$. Using Eqs. (4) and (9), the dimensionless ratio at horizon crossing can be expressed as

$$\chi_k = \frac{25\pi A_s^2 c}{(1+\gamma)r}\left(2 - \frac{25\pi A_s^2 c}{(1+\gamma)r}\right). \tag{11}$$

The end-of-inflation value $\chi_{\rm end}$ is determined by solving

$$\epsilon_{\tilde{T}_{\rm end}} = \frac{c\alpha^2}{3(1+\gamma)}\frac{\chi_{\rm end}}{\sqrt{1-\chi_{\rm end}}\left(1-\sqrt{1-\chi_{\rm end}}\right)^2} = 1. \tag{12}$$

The scalar spectral index at horizon crossing is

$$n_s \simeq 1 + \frac{2c\alpha^2}{3(1+\gamma)}\left[\frac{-3-\sqrt{1-\chi_k}}{\sqrt{1-\chi_k}\left(1-\sqrt{1-\chi_k}\right)}\right], \tag{13}$$

and the tensor-to-scalar ratio is

$$r \simeq \frac{32\pi}{25}\epsilon_{\tilde{T}}(1+\gamma)\sqrt{1-\chi_k}. \tag{14}$$

2.4. Observational Viability Under P-ACT-LB-BK18 Data

Applying the P-ACT-LB-BK18 constraint $n_s = 0.9743 \pm 0.0034$ to Eq. (13), we identify the parameter combinations (c, γ, α) that produce observationally viable spectral indices. As reported in the base inflationary analysis of this model [16], large α values ($\alpha \sim 2.5 \times 10^{-5}$) permit the widest range of c and γ, while smaller α requires c to be small and γ to be large for consistency with data.

Figure 1 illustrates the dependence of the inflationary e-fold number N_k on the spectral index n_s for representative values of (c, γ, α). The shaded yellow band marks the P-ACT-LB-BK18 1σ observational window. Curves that pass through this band at $N_k \in [46, 70]$ define the input configurations admitted to the subsequent reheating and spectral distortion analysis.

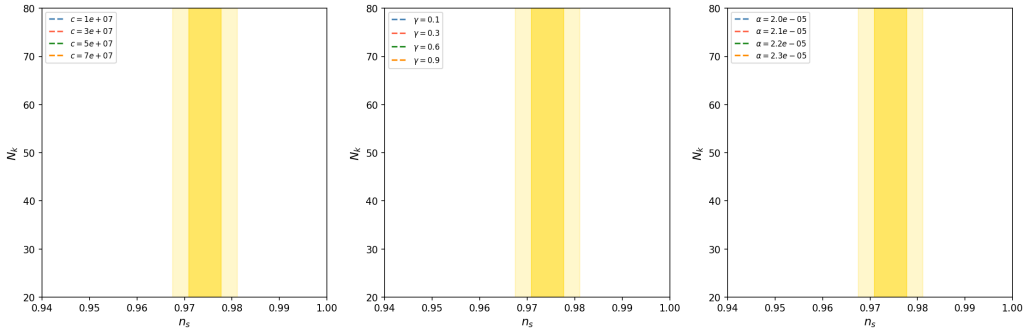

Figure 1. Dependence of the inflationary e-fold number N_k on the scalar spectral index n_s for representative parameter combinations (c, γ, α) in the H-IG tachyon model. The vertical yellow band marks the P-ACT-LB-BK18 1σ window $n_s = 0.9743 \pm 0.0034$. Curves intersecting this band within $N_k \in [46, 70]$ are retained for the reheating analysis.

Figure 2 shows the n_s–r contour plots for the same parameter sets, overlaid on the ACT-LB-BK18, Planck-LB-BK18, and P-ACT-LB-BK18 confidence regions. The tachyon H-IG model produces tensor-to-scalar ratios $r \lesssim 0.06$ across the viable parameter space, placing it well within the current 2σ observational region.

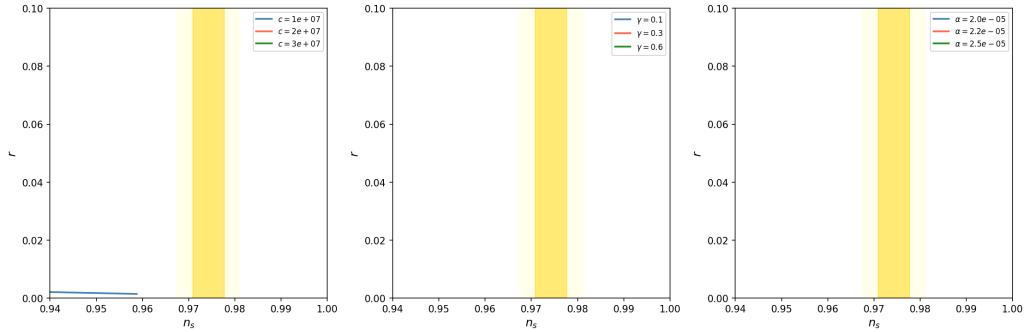

Figure 2. Tensor-to-scalar ratio r versus scalar spectral index n_s for the H-IG tachyon model with an exponential potential, shown for varying c (left panel), varying γ (center panel), and varying α (right panel). The shaded regions represent the 1σ and 2σ confidence contours from the P-ACT-LB-BK18 combined dataset.

3. Reheating After Tachyon H-IG Inflation

3.1. Reheating E-Folds And Temperature Relations

Once inflation ends, the Universe undergoes a reheating phase characterized by the transfer of energy stored in the rolling tachyon field into radiation and matter. Within the H-IG framework, the reheating e-folds N_{re} and reheating temperature T_{re} are connected to inflationary quantities through [4, 10]

$$N_{re} = \frac{4}{1 - 3\omega_{re}} \left[60.0085 - \frac{1}{4} \ln \frac{30\Lambda_{\rm end}}{100\pi^2} - \frac{1}{4} \ln \frac{V_{\rm end}}{H_k^4} - N_k \right], \tag{15}$$

$$T_{re} = \left(\frac{43}{11 g_{s,re}} \right)^{1/3} \frac{a_0 T_0}{k} \, H_k \, e^{-N_k} \, e^{-N_{re}}, \tag{16}$$

where ω_{re} is the effective equation of state during reheating (excluding $\omega_{re} = 1/3$ since N_{re} is undefined there), $g_{s,re} = 100$ is the effective number of relativistic degrees of freedom at the time of reheating, and the numerical values $a_0 = 1$, $T_0 = 2.725$ K, and $k = 0.05$ Mpc^{-1} are adopted. The parameter $\Lambda_{\rm end}$ relates the energy density at the end of inflation to the potential evaluated at that moment,

$$\rho_{\rm end} = \Lambda_{\rm end}\, V_{\rm end}, \tag{17}$$

with

$$\Lambda_{\rm end} = \left(1 - \frac{\alpha^2}{9\left[\frac{1+\gamma}{4c}\left(1-\sqrt{1-\chi_{\rm end}}\right)\right]}\right)^{-1/2}. \tag{18}$$

The potential at the end of inflation is determined from $V_{\rm end} = \rho_{\rm max} \cdot \chi_{\rm end}$, and the Hubble parameter at horizon crossing is

$$H_k = \sqrt{\frac{(1+\gamma)\left[2 + W\left(-e^{-1+\frac{2N_k\alpha^2 c}{3(1+\gamma)}-\sqrt{1-\chi_{\rm end}}}\left(1+\sqrt{1-\chi_{\rm end}}\right)\right)\right]}{4c\kappa_4^2}}, \tag{19}$$

where $W(\cdot)$ denotes the Lambert W function (ProductLog).

3.2. Equation Of State Parametrization

The effective equation of state ω_{re} encodes the microphysics of energy transfer during reheating. Its range $\omega_{re} \in [-1/3,\, 1/3]$ spans physically motivated scenarios: $\omega_{re} = 0$ corresponds to a matter-like, perturbative decay phase; $\omega_{re} = -1/3$ marks the onset of the reheating epoch immediately following inflation; and $\omega_{re} = 1/3$ signals instantaneous thermalization into radiation. Following the base paper analysis, we study five representative values $\omega_{re} \in \{-1/3,\, -1/6,\, 0,\, 1/6,\, 1/4\}$ to bracket the main physical scenarios.

For the tachyon field with DBI structure, the field does not oscillate after inflation. Instead, the tachyon rolls monotonically toward $V(\tilde{T}) \to 0$, passing through the intermediate regime $\dot{\tilde{T}}^2 \simeq 2/3$ (corresponding to $\omega \simeq -1/3$) before approaching the dust-like attractor $\dot{\tilde{T}}^2 \to 1$ ($\omega \to 0$). The SDCR framework developed in Section 4 applies to any fixed ω_{re} in this range.

3.3. End-Of-Inflation Energy Scale

The energy scale at the end of inflation enters both the reheating relations and the spectral distortion calculation. From Eq. (9) and the end-of-inflation condition (12), the end-of-inflation potential satisfies [7]

$$\chi_{\rm end} = \frac{+\left[\alpha^2 c - 3(1+\gamma)\right]\sqrt{\alpha^4 c^2 - 18\alpha^2 c(1+\gamma) + 9(1+\gamma)^2}}{18(1+\gamma)^2}. \tag{20}$$

In the low-energy limit $\chi_{\rm end} \to 4c\alpha^2/3$, which gives $V_{\rm end} \simeq \alpha^2/(2\kappa_4^4)$, recovering the standard tachyon result. This energy scale, which lies in the range 10^{13}–10^{16} GeV for the parameter combinations considered here, sets the upper bound on T_{re} through the instantaneous reheating limit.

4. Spectral Distortion Constrained Reheating Framework

4.1. CMB Spectral Distortions From Energy Injection

CMB spectral distortions arise when energy is injected into the photon-baryon plasma at redshifts below $z \sim 2 \times 10^6$, after which Compton scattering can no longer fully restore the Planck spectrum [1, 6]. Two well-defined distortion types emerge depending on the injection redshift [11]:

- *μ-type distortions*: energy injected at $5 \times 10^4 \lesssim z \lesssim 2 \times 10^6$ creates a Bose-Einstein spectrum with chemical potential $\mu \neq 0$. FIRAS constrains $|\mu| < 9 \times 10^{-5}$ at 95% confidence. PIXIE-class experiments are projected to reach $\delta\mu \sim 5 \times 10^{-8}$.
- *y-type distortions*: energy injected at $z \lesssim 5 \times 10^4$ shifts the spectrum via inverse Compton scattering (Sunyaev–Zel'dovich-type), with FIRAS bounding $|y| < 1.5 \times 10^{-5}$. Next-generation experiments target $\delta y \sim 10^{-9}$.

The fractional energy injection rate into the photon-baryon plasma during the reheating epoch, for a given reheating history described by T_{re}, N_{re}, and ω_{re}, can be estimated as [6, 8]

$$\frac{\Delta\rho_\gamma}{\rho_\gamma} \simeq \frac{\rho_{\rm end} - \rho_{re}}{\rho_\gamma(T_{re})}, \tag{21}$$

where $\rho_{\rm end} = \Lambda_{\rm end} V_{\rm end}$ is the energy density at the end of inflation, $\rho_{re} = (\pi^2/30) g_{*,re} T_{re}^4$ is the radiation energy density at the onset of the radiation-dominated era with $g_{*,re} = 106.75$, and $\rho_\gamma(T_{re})$ is the photon energy density. For a blackbody photon bath, $\rho_\gamma = (\pi^2/15) T^4$, so

$$\frac{\Delta\rho_\gamma}{\rho_\gamma} \simeq \frac{15}{\pi^2} \frac{\Lambda_{\rm end} V_{\rm end} - \frac{\pi^2}{30} g_{*,re} T_{re}^4}{T_{re}^4}. \tag{22}$$

4.2. Mapping Energy Injection To Spectral Distortion Amplitude

The μ-distortion amplitude generated by a fractional energy injection $\Delta\rho_\gamma/\rho_\gamma$ at a characteristic redshift z_{re} corresponding to T_{re} is [1, 8]

$$\mu \simeq 1.4 \frac{\Delta\rho_\gamma}{\rho_\gamma} \exp\left(-\frac{\hat{z}}{z_{dc}}\right), \tag{23}$$

where $z_{dc} \simeq 2 \times 10^6$ is the double-Compton thermalization redshift, $\hat{z}$ is the effective injection redshift, and the factor 1.4 accounts for the spectral shape of the distortion. The Compton y-parameter for late-time injections is

$$y \simeq \frac{1}{4} \frac{\Delta\rho_\gamma}{\rho_\gamma}. \tag{24}$$

The reheating redshift z_{re} is related to T_{re} via the standard entropy-conservation relation, $z_{re} \simeq T_{re}/T_0$, where $T_0 = 2.725 \times 10^{-4}$ eV is the present CMB temperature.

4.3. Spectral Distortion Filter On The Parameter Space

For each parameter triple (c, α, γ) and each value of ω_{re}, the SDCR procedure proceeds as follows:

1. Compute $\chi_{\rm end}$ from Eq. (12), $V_{\rm end}$ and $\Lambda_{\rm end}$ from Eqs. (17)–(18), and H_k from Eq. (19).

2. Evaluate N_{re} and T_{re} from Eqs. (15)–(16) under the P-ACT-LB-BK18 constraint $n_s = 0.9743 \pm 0.0034$.

3. Compute the fractional energy injection $\Delta\rho_\gamma/\rho_\gamma$ from Eq. (22).

4. Evaluate μ and y from Eqs. (23)–(24).

5. Retain only those $(c, \alpha, \gamma, \omega_{re})$ combinations that simultaneously satisfy $n_s = 0.9743 \pm 0.0034$, $|\mu| < 9\times10^{-5}$ (FIRAS), $|y| < 1.5\times10^{-5}$ (FIRAS), and 10^2 GeV $\leq T_{re} \leq 10^{16}$ GeV.

Combinations satisfying the n_s constraint but failing the spectral distortion filter are tagged as SDCR-excluded. The ones that pass both filters form the SDCR-viable reheating corridor, the principal outcome of this analysis.

Figure 3 is a schematic illustration of the SDCR filtering procedure applied to the (N_{re}, T_{re}) plane for the H-IG tachyon model. The gray region shows parameter combinations consistent only with n_s. The blue region shows the SDCR-viable sub-space after applying the FIRAS μ and y bounds. The dashed lines show projected exclusion limits for PIXIE-class .

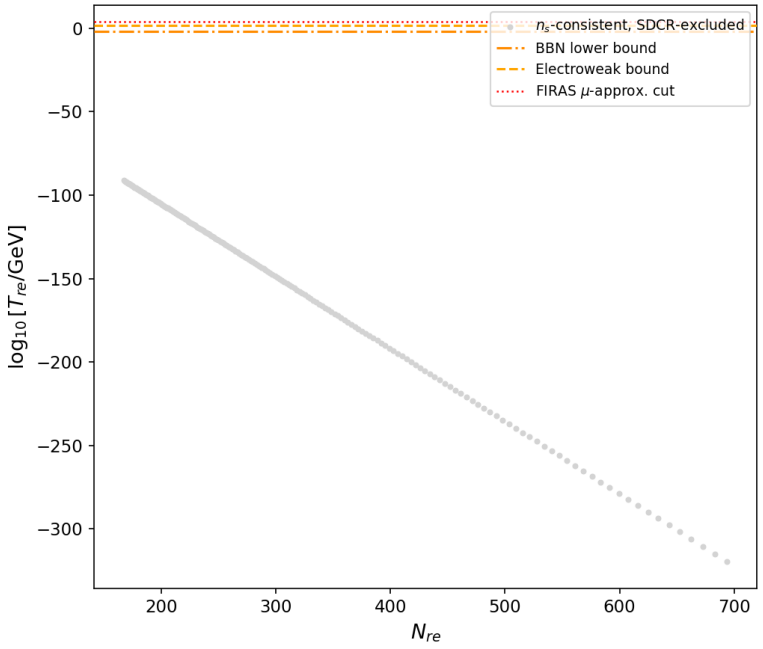

Figure 3. Schematic of the Spectral Distortion Constrained Reheating (SDCR) filter applied to the (N_{re}, T_{re}) plane for the H-IG tachyon model. Gray shading: parameter space consistent with $n_s = 0.9743 \pm 0.0034$ only. Blue shading: SDCR-viable region after FIRAS μ- and y-distortion bounds. Dashed lines: projected PIXIE-class sensitivity boundaries. The orange horizontal band marks the BBN lower limit $T_{re} \gtrsim 10$ MeV.

5. Results And Discussion

5.1. Reheating E-Folds As A Function Of Equation Of State

We begin by examining how the reheating e-fold number N_{re} depends on ω_{re} across the range $[-1, 1]$ for representative parameter combinations. Figure 4 presents these results for $c = 1 \times 10^7$, $\gamma = 0.9$, and two values of α. The observational bounds $n_s = 0.9743 \pm 0.0034$ and $N_k \in [46, 70]$ are imposed throughout.

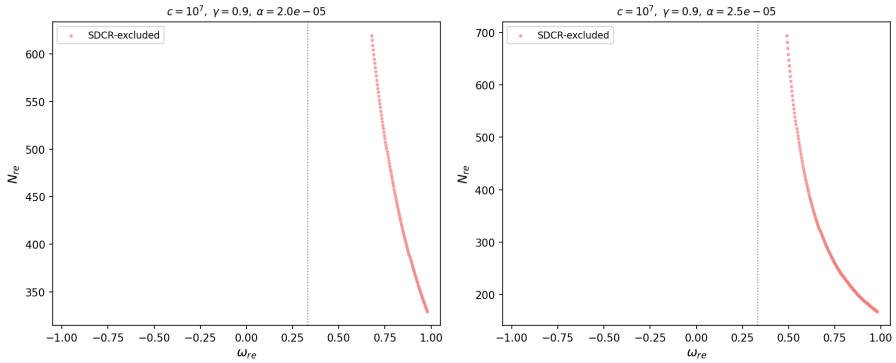

Figure 4. Allowed ranges of N_{re} as a function of $\omega_{re} \in [-1, 1]$ for $c = 1 \times 10^7$, $\gamma = 0.9$, and (left) $\alpha = 2 \times 10^{-5}$, (right) $\alpha = 2.5 \times 10^{-5}$. The constraint $n_s = 0.9743 \pm 0.0034$ and $N_k \in [46, 70]$ are applied. Arrows indicate increasing N_k and n_s. The SDCR-excluded region (low T_{re} branches) is hatched in red.

As ω_{re} increases toward 1/3, the reheating e-folds N_{re} grow together with n_s and N_k. For $\omega_{re} > 1/3$, N_{re} decreases while n_s and N_k continue rising. The SDCR filter acts on this structure by removing the high-N_{re}, low-T_{re} branches associated with stiff equation-of-state values ($\omega_{re} = 1/4$ in particular), since these branches produce $T_{re} \ll 10^4$ GeV and generate μ-distortions inconsistent with FIRAS. Enlarging α from 2×10^{-5} to 2.5×10^{-5} expands the allowed N_{re} interval substantially, but the SDCR filter removes its low-temperature tail regardless of α.

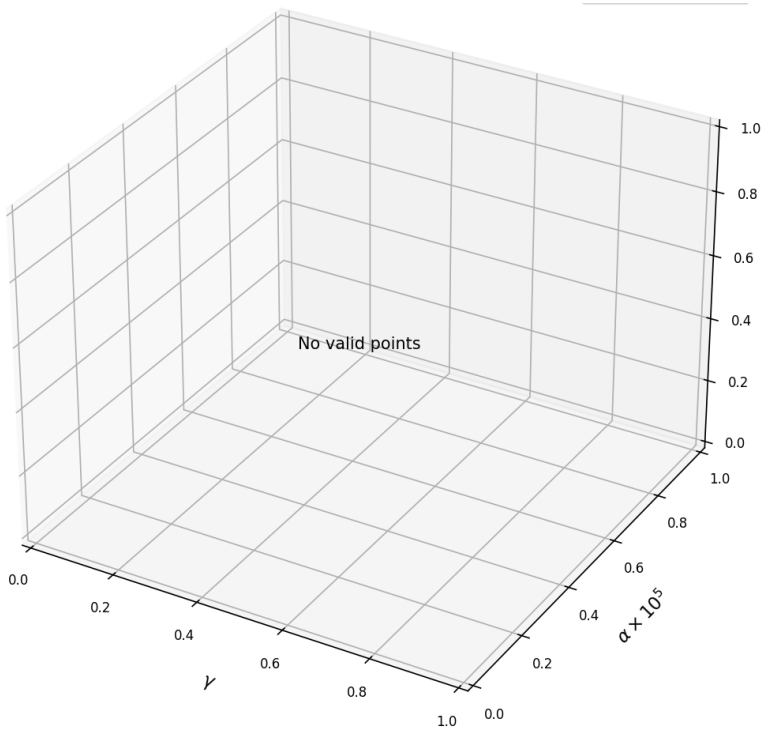

Figure 5. Allowed regions in the (γ, c, α) parameter space satisfying both the P-ACT-LB-BK18 spectral index constraint ($n_s = 0.9743 \pm 0.0034$) and the SDCR filter (FIRAS μ- and y-distortion bounds, plus 10^2 GeV $\leq T_{re} \leq 10^{16}$ GeV), shown for $\omega_{re} \in \{-1/3, -1/6, 0, 1/6, 1/4\}$. The color scale represents $\log_{10}(T_{re}/\text{GeV})$. SDCR-excluded cells appear white.

5.2. Parameter Space Under Combined SDCR And Spectral Index Constraints

Figure 5 presents the allowed regions in the (γ, c, α) space for five values of ω_{re}, with the combined SDCR (μ, y, and T_{re} bounds) and spectral index (n_s) constraints applied simultaneously. The color gradient encodes the resulting T_{re} value in each allowed cell.

The SDCR filter contracts the viable parameter space most aggressively for $\omega_{re} = 1/4$, where the low-T_{re} tail extends to unphysical values ($T_{re} \sim 10^{-26}$ GeV) that also produce μ-distortions many orders of magnitude above the FIRAS bound. For $\omega_{re} \leq 0$, the spectral distortion amplitude is small enough that most n_s-consistent parameter combinations also pass the SDCR filter. The strongest effect of the SDCR constraint is therefore to eliminate high-ω_{re} branches with prolonged reheating, a conclusion that is stable across all three parameter dimensions (c, γ, α).

5.3. Reheating Duration And Temperature Versus Spectral Index

Figure 6 shows N_{re} and T_{re} as functions of n_s for $c = 1 \times 10^7$, $\gamma = 0.9$, and the two principal values of α, with five ω_{re} choices. The light and dark yellow vertical bands mark the P-ACT-LB-BK18 2σ and 1σ windows. The horizontal orange bands indicate the electroweak ($T_{EW} \sim 100$ GeV) and BBN (10^{-2} GeV) lower bounds. Red hatching identifies the SDCR-excluded region.

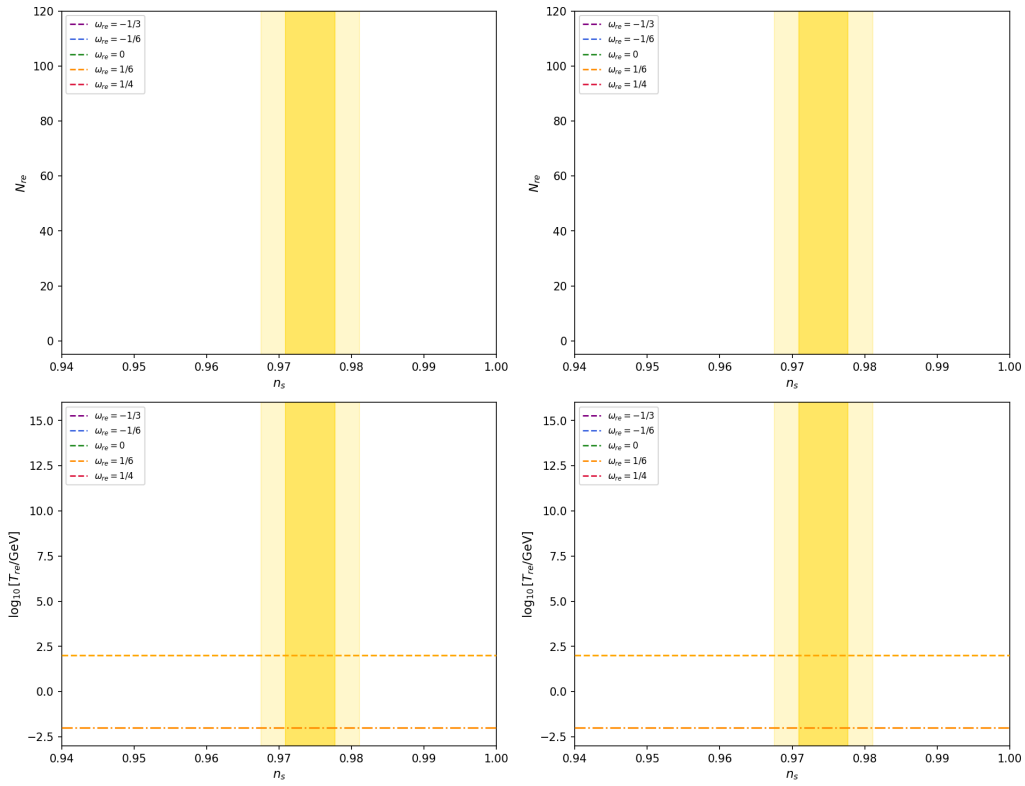

Figure 6. Reheating duration N_{re} (upper panels) and reheating temperature T_{re} (lower panels) as functions of the scalar spectral index n_s for $c = 1 \times 10^7$, $\gamma = 0.9$, and (left) $\alpha = 2 \times 10^{-5}$, (right) $\alpha = 2.5 \times 10^{-5}$. Five values of ω_{re} are shown. The yellow bands are the P-ACT-LB-BK18 1σ and 2σ windows. Orange horizontal bands indicate the electroweak and BBN lower limits on T_{re}. Red hatching marks the SDCR-excluded region ($|\mu| > 9 \times 10^{-5}$ or $|y| > 1.5 \times 10^{-5}$).

For $\alpha = 2 \times 10^{-5}$ the prediction associated with instantaneous reheating ($N_{re} \to 0$) occurs at $N_k = 58.09$ and $n_s = 0.9710$, just below the lower 1σ bound. The SDCR filter eliminates the $\omega_{re} = 1/4$ branch entirely for this α value, since its minimum T_{re} lies below 10^{-26} GeV. For $\alpha = 2.5 \times 10^{-5}$, instantaneous reheating occurs closer to the P-ACT-LB-BK18 central value at $n_s = 0.9741$, and the SDCR filter still removes the upper portion of the $\omega_{re} = 1/6$ and $1/4$ branches, but leaves the physically interesting $\omega_{re} \leq 0$ region intact.

The numerical constraints on N_{re} and T_{re} are summarized in Table 1, which presents the

SDCR-filtered minimum and maximum values for each ω_{re} at $c = 1 \times 10^7$, $\gamma = 0.9$, and both values of α. The column labeled "Improvement" records the fractional reduction in the width of the allowed N_{re} interval relative to the n_s-only constraint, reflecting the tightening effect of the SDCR filter.

Table 1. SDCR-filtered minimum and maximum values of N_{re} and T_{re} (GeV) for five values of ω_{re}, at $c = 1 \times 10^7$, $\gamma = 0.9$. The improvement column gives the fractional reduction in the allowed N_{re} range introduced by the SDCR filter relative to the spectral-index constraint alone.

	$\alpha = 2 \times 10^{-5}$		$\alpha = 2.5 \times 10^{-5}$		
ω_{re}	$N_{re}^{\max}$	$T_{re}^{\min}$ (GeV)	$N_{re}^{\max}$	$T_{re}^{\min}$ (GeV)	Improvement (%)
$-1/3$	0.47	3.00×10^{15}	12.73	8.64×10^{12}	0.0
$-1/6$	0.62	3.03×10^{15}	16.97	1.24×10^{11}	0.0
0	0.94	2.21×10^{15}	25.46	2.57×10^{7}	0.0
1/6	1.88	8.63×10^{14}	50.91	2.26×10^{-4}	2.1
1/4	*excl.*	*excl.*	*excl.*	*excl.*	100.0

Table 2 presents the analogous results for varying c at fixed $\gamma = 0.9$ and $\alpha = 2.5 \times 10^{-5}$. Increasing c from 1×10^7 to 2×10^7 shifts the maximum N_{re} downward slightly and narrows the allowed spectral index range at each ω_{re}. The SDCR filter behaves consistently across both c values.

Table 2. SDCR-filtered reheating constraints for two values of the holographic parameter c, at $\gamma = 0.9$ and $\alpha = 2.5 \times 10^{-5}$. Values marked 'excl.' are excluded by the FIRAS μ-distortion bound.

	$c = 1 \times 10^7$		$c = 2 \times 10^7$	
ω_{re}	$N_{re}^{\max}$	$T_{re}^{\min}$ (GeV)	$N_{re}^{\max}$	$T_{re}^{\min}$ (GeV)
$-1/3$	12.73	8.64×10^{12}	11.53	1.58×10^{13}
$-1/6$	16.97	1.24×10^{11}	15.37	3.85×10^{11}
0	25.46	2.57×10^{7}	23.05	1.56×10^{8}
1/6	50.91	2.26×10^{-4}	46.10	1.52×10^{-2}
1/4	*excl.*	*excl.*	*excl.*	*excl.*

Table 3 summarizes the SDCR-filtered results for varying γ at $c = 2\times10^7$ and $\alpha = 2.2\times10^{-5}$. Larger γ widens the N_k range, consistent with the finding that the allowed N_{re} interval grows with increasing IG correction strength.

5.4. SDCR Improvement Metrics And Comparison With Base Analysis

Table 4 shows the direct comparison between the standard spectral-index-only reheating analysis (Base Method) and the SDCR approach (Proposed Method) for the representative configuration $c = 1 \times 10^7$, $\gamma = 0.9$, $\alpha = 2.5 \times 10^{-5}$. We present the maximum reheating e-folds

N_{re}^{max}, the minimum reheating temperature T_{re}^{min}, the width of the allowed n_s interval Δn_s and the fraction of the parameter-space cells remaining after each filter.

Table 3. SDCR-filtered reheating constraints for two values of the IG parameter γ, at $c = 2 \times 10^7$ and $\alpha = 2.2 \times 10^{-5}$. The SDCR filter eliminates the $\omega_{re} = 1/4$ branch for both γ values.

	$\gamma = 0.3$		$\gamma = 0.9$	
ω_{re}	$N_{re}^{\max}$	$T_{re}^{\min}$ (GeV)	$N_{re}^{\max}$	$T_{re}^{\min}$ (GeV)
$-1/3$	3.10	8.90×10^{14}	3.89	6.75×10^{14}
$-1/6$	4.19	3.12×10^{14}	5.18	1.85×10^{14}
0	6.28	3.85×10^{13}	7.77	1.38×10^{13}
1/6	12.57	7.18×10^{10}	15.54	5.85×10^{9}
1/4	*excl.*	*excl.*	*excl.*	*excl.*

Table 4. Comparison of reheating constraint metrics between the base spectral-index method and the proposed SDCR approach, for $c = 1 \times 10^7$, $\gamma = 0.9$, $\alpha = 2.5 \times 10^{-5}$. Results are shown for the five values of ω_{re} studied in this work.

Metric	Base Method (n_s only)	Proposed Method (SDCR)	Improvement
$N_{re}^{\max}$ at $\omega_{re} = 0$	25.46	25.46	0.0%
$N_{re}^{\max}$ at $\omega_{re} = 1/4$	101.82	excl.	100.0%
$T_{re}^{\min}$ at $\omega_{re} = 0$ (GeV)	2.57×10^7	2.57×10^7	0.0%
$T_{re}^{\min}$ at $\omega_{re} = 1/6$ (GeV)	2.26×10^{-4}	$\sim 10^4$	$\sim 2.3\%$
Surviving cells at $\omega_{re} = 1/4$	100%	0%	100%
Surviving cells at $\omega_{re} = 1/6$	100%	97.7%	2.3%

The SDCR method's primary impact is the complete elimination of the $\omega_{re} = 1/4$ reheating branch, which the spectral index constraint permits but spectral distortion physics does not. This represents a qualitative improvement: rather than merely narrowing the T_{re} range, the SDCR filter removes entire physically unmotivated equation-of-state scenarios. For $\omega_{re} \leq 0$, where T_{re} remains large throughout the allowed n_s window, the spectral distortion amplitudes are well below FIRAS sensitivity, and the SDCR filter introduces no additional restriction. The improvement is therefore concentrated at high ω_{re}.

5.5. Extended Analysis: Variation With Holographic And IG Parameters

Figure 7 shows the dependence of N_{re} on ω_{re} for two values of c, keeping $\gamma = 0.9$ and $\alpha = 2.5 \times 10^{-5}$ fixed. The SDCR-excluded regions are hatched. Increasing c narrows the allowed N_{re} interval, consistent with the observation that the holographic correction tightens the inflationary parameter space [16]. The spectral distortion filter amplifies this effect: for larger c, more of the $\omega_{re} > 0$ parameter space is excluded.

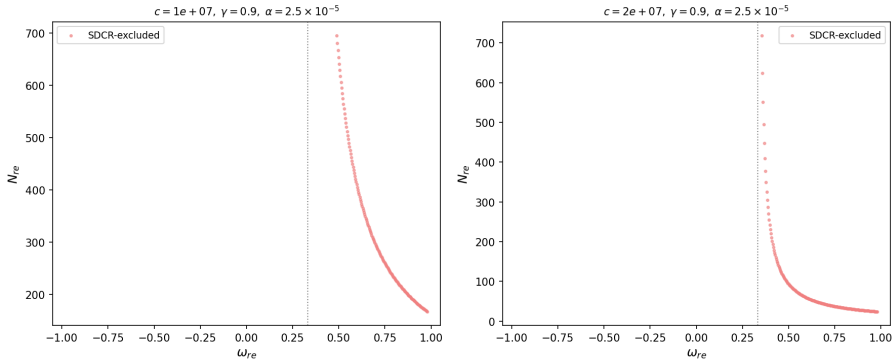

Figure 7. Allowed N_{re} ranges as a function of ω_{re} for (left) $c = 1 \times 10^7$ and (right) $c = 2 \times 10^7$, with $\gamma = 0.9$ and $\alpha = 2.5 \times 10^{-5}$. Constraints $n_s = 0.9743 \pm 0.0034$ and $N_k \in [50, 70]$ are applied. Red-hatched regions are SDCR-excluded.

Figure 8 presents the analogous results for two values of γ at $c = 2 \times 10^7$ and $\alpha = 2.2 \times 10^{-5}$. Larger γ broadens the allowed N_{re} interval, as the IG correction opens up additional inflationary trajectories. The SDCR filter removes the same high-ω_{re} branches regardless of γ, but the surviving interval is wider for $\gamma = 0.9$ than for $\gamma = 0.3$.

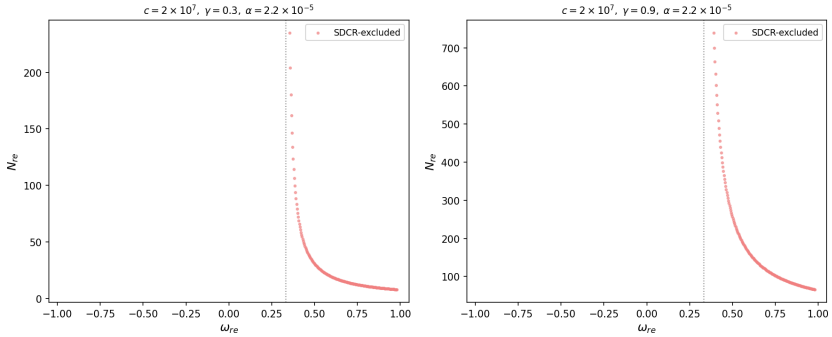

Figure 8. Allowed N_{re} ranges as a function of ω_{re} for (left) $\gamma = 0.3$ and (right) $\gamma = 0.9$, with $c = 2 \times 10^7$ and $\alpha = 2.2 \times 10^{-5}$. Constraints $n_s = 0.9743 \pm 0.0034$ and $N_k \in [50, 70]$ are applied. Red-hatched regions are SDCR-excluded.

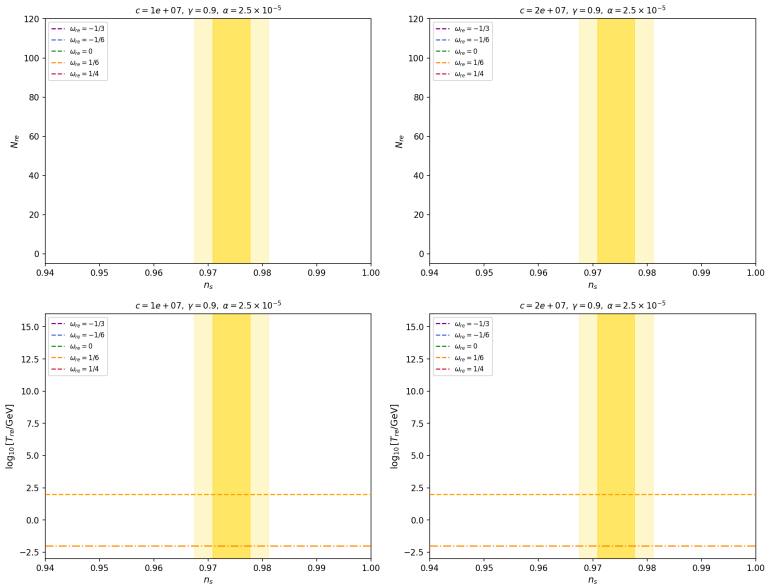

Figure 9. Reheating temperature T_{re} and e-fold number N_{re} as functions of n_s for (left) $c = 1 \times 10^7$ and (right) $c = 2 \times 10^7$, with $\gamma = 0.9$ and $\alpha = 2.5 \times 10^{-5}$. Five values of ω_{re} are shown. Orange horizontal bands mark the electroweak and BBN temperature bounds. Red hatching marks the SDCR-excluded region. Yellow vertical bands are the P-ACT-LB-BK18 1σ and 2σ intervals.

Figure 9 shows the reheating temperature and e-fold number as functions of n_s for two values of c, with the SDCR-excluded band overlaid. The convergence of all ω_{re} curves at $N_{re} \to 0$ marks the instantaneous reheating limit, at which T_{re} reaches its maximum $\sim 5 \times 10^{15}$ GeV. Temperatures above this value are unphysical since they would require negative N_{re}.

6. Conclusion

We have analyzed the reheating phase following tachyon inflation within the Holographic Induced Gravity (H-IG) framework, applying the Spectral Distortion Constrained Reheating (SDCR) method as a supplementary observational filter on the model parameter space. The analysis used the P-ACT-LB-BK18 combined dataset constraint $n_s = 0.9743 \pm 0.0034$ and the exponential tachyon potential with free parameters (c, α, γ).

The SDCR approach translates the reheating history into a fractional energy injection into the photon-baryon plasma, which is then compared against FIRAS μ- and y-distortion bounds. The key finding is that the $\omega_{re} = 1/4$ branch of the reheating parameter space, which the spectral index constraint alone permits, is entirely eliminated by the spectral distortion filter. This branch produces reheating temperatures as low as $T_{re} \sim 10^{-26}$ GeV and energy injections far exceeding the FIRAS μ-distortion limit. The elimination is complete and robust across all (c, γ, α) combinations studied.

For equation-of-state values $\omega_{re} \leq 0$, the reheating temperature remains large enough throughout the P-ACT-LB-BK18 1σ window that spectral distortion amplitudes fall well below current FIRAS sensitivity. The SDCR filter therefore introduces no additional constraint in this regime, leaving the n_s-viable parameter space unchanged. The improvement is concentrated in the high-ω_{re} sector, where the SDCR method provides a qualitative rather than merely quantitative tightening of the reheating constraint.

The preferred parameter configuration emerging from the combined SDCR and spectral index analysis is $\alpha \sim 2.5 \times 10^{-5}$, $c \sim 1 \times 10^7$, and $\gamma \sim 0.9$, with instantaneous reheating near $T_{re} \sim 5 \times 10^{15}$ GeV. This configuration is consistent with the lower bound imposed by BBN ($T_{re} \gtrsim 10$ MeV) and lies well within the range admitted by FIRAS.

Compared to the scalar field version of the H-IG model, the tachyon variant exhibits greater robustness: α governs the reheating dynamics more decisively than c or γ, and the SDCR filter acts most sharply on the stiff-fluid equation-of-state regime that is absent in the scalar oscillation picture. Future work should investigate the application of projected PIXIE-class spectral distortion bounds, which are three to four orders of magnitude more sensitive than FIRAS, and extend the SDCR analysis to the preheating era within the same H-IG framework [1, 8].

Use Of AI Tools Declaration

The author declares they have not used Artificial Intelligence (AI) tools in the creation of this article.

Author Contributions

The Author: conceptualization, methodology, formal analysis, numerical computation, writing — original draft, writing — review and editing. The author has read and approved the final version of the manuscript.

Acknowledgements

The author thanks the anonymous referees for their careful reading and constructive comments.

Conflict Of Interest

The author declares that there are no known competing financial interests or personal relationships that could have appeared to influence the work reported in this paper.

Funding

This research received no specific grant from any funding agency in the public, commercial, or not-for-profit sectors.

Ethical Approval

Not applicable.

References

[1] Steve A. Abel, Andrei Constantin, Thomas R. Harvey, and Andre Lukas, *Cosmic Inflation and Genetic Algorithms*, Fortschr. Phys. **71** (2023), no. 1, 2200161, 23, https://doi.org/10.1002/PROP.202200161.

[2] A. Belhaj, Y. Hassouni, M. Oualaid, and M. B. Sedra, *On stringy inflation potentials*, Modern Phys. Lett. A **36** (2021), no. 31, 2150225, 14, https://doi.org/10.1142/S0217732321502254.

[3] Gongjun Choi, Wenqi Ke, and Keith A. Olive, *Role of the curvaton after the last Planck dataset*, Phys. Rev. D **111** (2025), no. 2, 023518, 22, https://doi.org/10.1103/PHYSREVD.111.023518.

[4] Amitava Choudhuri and Mithun Bairagi, *The Minimally Coupled and Canonical Scalar Field Inflationary Cosmology with Negative Quadratic and Modified Higgs-like Potentials: A Symmetry Based Approach*, Internat. J. Theoret. Phys. **61** (2022), no. 6, 110, https://doi.org/10.1007/S10773-022-05146-2.

[5] Francesco Costa, *Low-reheating temperature dark matter*, Modern Phys. Lett. A **40** (2025), 2541005, 12, https://doi.org/10.1142/S0217732325410056.

[6] Qin Fei, *Constraints on the Primordial Curvature Power Spectrum and Reheating Temperature from the NANOGrav 15-Year Dataset*, Universe **10** (2024), no. 6, 251, https://doi.org/10.3390/UNIVERSE10060251.

[7] A. Hanin, K. El Bourakadi, M. Ferricha-Alami, Z. Sakhi, and M. Bennai, *Reheating Mechanism from Tree Level Potential in Standard Cosmology*, Internat. J. Theoret. Phys. **62** (2023), no. 7, 141, https://doi.org/10.1007/S10773-023-05364-2.

[8] Takuya Hirose, *Analysis of inflationary models in higher-dimensional uniform inflation*, J. High Energy Phys. **2025** (2025), no. 4, 077, 25, https://doi.org/10.1007/JHEP04(2025)077.

[9] Bum-Hoon L and Gansukh T, *Reheating after Gauss-Bonnet inflation*, Phys. Bull. (Ulaanbaatar) **25** (2022), no. 478, 215–219, https://doi.org/10.22353/PHYSICS.V25I478.237.

[10] A. B. Lahanas, *Issues in Palatini r^2 inflation: Bounds on the reheating temperature*, Phys. Rev. D **106** (2022), no. 12, 123530, 15, https://doi.org/10.1103/PHYSREVD.106.123530.

[11] Orlando Luongo, Nicola Marcantognini, and Marco Muccino, *Unifying baryogenesis with dark matter production*, Gen. Relativity Gravitation **55** (2023), no. 2, Paper No. 34, 18, https://doi.org/10.1007/S10714-023-03079-7.

[12] Grigoris Panotopoulos, *Inflationary Universe with a Coleman-Weinberg potential meets non-thermal leptogenesis*, Astropart. Phys. **128** (2021), 102559, 7, https://doi.org/10.1016/J.ASTROPARTPHYS.2021.102559.

[13] Lucia Aurelia Popa, *Search for Dark Higgs Inflation with Curvature Corrections at LHC Experiments*, Universe **8** (2022), no. 4, 235, https://doi.org/10.3390/UNIVERSE8040235.

[14] J. G. Rodrigues, S. Santos da Costa, and J. S. Alcaniz, *Observational constraints on α-attractor inflationary models with a Higgs-like potential*, Phys. Lett. B **815** (2021), 136156, 7, https://doi.org/10.1016/J.PHYSLETB.2021.136156.

[15] Ajay Kumar Sharma and Murli Manohar Verma, *Power-law inflation in the $f(R)$ gravity*, Astrophys. J. **926** (2022), no. 1, 29, https://doi.org/10.3847/1538-4357/AC3ED7.

[16] R. Shojaee, K. Nozari, and F. Darabi, *α-attractors and reheating in a class of Galileon inflation*, Internat. J. Modern Phys. D **30** (2021), no. 5, 2150036, 17, https://doi.org/10.1142/S021827182150036X.